
SEMI-SUPERVISED ATMOSPHERIC COMPONENT LEARNING IN LOW LIGHT IMAGE PROBLEM

Masud An Nur Islam Fahim
Chosun University
Gwangju, South Korea
mostofafahim21@gmail.com

Nazmus Saqib
Chosun University
Gwangju, South Korea
nsaqib1995@gmail.com

Jung Ho Yub
Chosun University
Gwangju, South Korea
junghoyub@gmail.com

April 18, 2022

ABSTRACT

Ambient lighting conditions play a crucial role in determining the perceptual quality of images from photographic devices. In general, inadequate transmission light and undesired atmospheric conditions jointly degrade the image quality. If we know the desired ambient factors associated with the given low-light image, we can recover the enhanced image easily [1]. Typical deep networks perform enhancement mappings without investigating the light distribution and color formulation properties. This leads to a lack of image instance-adaptive performance in practice. On the other hand, physical model-driven schemes suffer from the need for inherent decompositions and multiple objective minimizations. Moreover, the above approaches are rarely data efficient or free of postprediction tuning. Influenced by the above issues, this study presents a semisupervised training method using no-reference image quality metrics for low-light image restoration. We incorporate the classical haze distribution model [2] to explore the physical properties of the given image in order to learn the effect of atmospheric components and minimize a single objective for restoration. We validate the performance of our network for six widely used low-light datasets. The experiments show that the proposed study achieves state-of-the-art or comparable performance.

1 Introduction

Images captured under limited lighting conditions exhibit lower contrast, inadequate detail, and unexpected noise. Recently available photographic devices can alleviate many of the problems, but they leave artifact traces such as noise, halos, or blurred contours. These artifacts can seriously degrade the performance of computer vision tasks apart from aesthetic issues. For example, underexposed images lead to unsatisfactory performances in tasks such as object detection, segmentation, and scene understanding [3].

Recent trends show that researchers have been focusing on developing new methods for image enhancement by blending physical models with end-to-end networks. In this context, Retinex theory [4, 5] is a well-known approach in solving conventional low-light enhancement problems. Early approaches used the handcrafted algorithm to decompose the input image into reflectance and illumination components, followed by a minimization step to obtain the optimal components which were then used to recover the enhanced image. The work on Retinex-net [6] made improvements by learning image decomposition adaptively for the given low-light images. However, the overall procedure has to learn the individual components and the associated optimization steps for proper reconstruction. As a result, the obtained solution often contains coarse illumination; hence, handcrafted postprocessing is required to reduce the artifacts.

Another enhancement approach [1], inspired by the hazy image recovery equation [7], directly estimates dark channels and bright channel priors for low light enhancement. However, these types of approaches also sometimes produce unwanted noise artifacts and improper color saturation. Even though the above approaches adopt physical models for image restoration, their underlying optimization procedures face difficult challenges involving multiple objective goals. Moreover, these methods [6] utilize manual adjustments before and after restoration. Lastly, their assumptions regarding image decomposition work well under certain lighting conditions but often lack broader generalization to handle image enhancement problems.

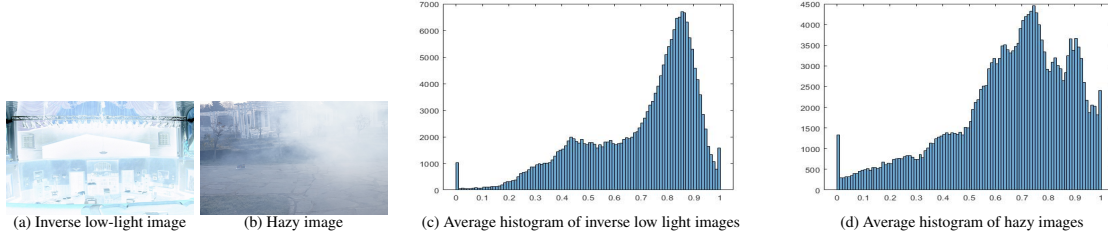


Figure 1: Here, we show the average histogram for the 40 random hazy images from [8] dataset and similar low-light photos from the GLADNet [9] dataset. After performing the inversion upon the low-light pictures, we can see similar trends in the histogram of the transformed and hazy images. This statistical phenomenon influenced the proposed study to incorporate haze distribution theory for image restoration.

To address the above concerns, we constructed a semi-supervised approach for learning the environmental constraints for image enhancement. We can trace the idea of integrating image dehazing theory into a low-light enhancement back to [10]. However, this earlier approach is deficient in numerous aspects, such as weak robustness and spatial fidelity. From the image haze formulation equation [7], we obtain the atmospheric light information and transmission matrix that jointly explain the haze in the natural images. We assume that low-light to hazy image transformation will enable us to incorporate the haze distribution equation. As a result, the linear inversion operation will perform the necessary transformation to produce a “hazy image” from the given low-light image [1].

Following this, our parameter space learns the atmospheric information and transmission matrix from the inverted image and solves the dehazing equation which in turn is followed by re-inversion to produce the enhanced output. The overall restoration procedure is free of any hand-crafted operations apart from image normalization. To avoid individual optimization procedures, we design a compact formulation for learning the ambient constraints altogether. In the overall training procedure, we use only 10% of the given labels for the proposed semi-supervised scheme. In essence, we propose a semi-supervised approach for learning the ambient factors from the given image through image haze distribution theory. The following summarize the significant contributions of this study:

- The proposed study uses an image quality assessment metric to regulate semi-supervised learning for low-light image restoration. This allows for only a fraction of the images having ground truths during training while achieving the desirable result.
- Our study investigates the common spatial degradation found in low-light enhancement and proposes an effective loss function combination that addresses the issues.
- Previous low-light enhancements tend to primarily rely on specific priors such as dark/bright channels, illumination, and reflection from the physical and environmental domains in order to obtain state-of-the-art results. In our study, no such priors are required to produce similar or better results.
- It is common in decomposition-based methods to rely on intensive manual postprocessing following inference. In contrast, our model can provide state-of-the-art end-to-end low-light enhancement without relying on such postprocessing.

The rest of the paper is organized as follows. Section 2 covers related works, and section 3 describes our proposed approach. In section 4, we present the detailed comparative analysis, and this is followed by the conclusion.

2 Related work

Optimization based methods. Traditional studies address the low-light enhancement challenge with the help of handcrafted optimization procedures or norm minimization methods. The optimization procedures, rely on assumptions, such as dark/bright channel priors [11, 10, 12]. Further, sub-optimal solutions are obtained using mathematical models

such as retinex theory [6] and multi-scale retinex theory [4, 5]. Some of the studies also use handcrafted fusion input [13, 14] instead of the original image.

Earlier retinex methods [4, 5] use Gaussian functions to maintain dynamic range compression and color consistency. Several optimization approaches estimate the illumination map by combining not only adaptive [15], bilateral [16, 17], guided [18], and bright-pass [19] filters but also derivation [10, 12] and structural assumptions [11]. Recently, to address the noise issue within retinex approaches, several methods have applied postprocessing steps such as noise fusion [20] or noise addition [21, 22]. Moreover, fusion-based approaches [1] employ background highlighting and multiple exposure information. In addition, multispectral image fusion combines the given image with an infrared image using a pseudo-fusion algorithm [23].

Despite the merits of the aforementioned methods, in general, their performance is not noise adaptive, contrast/instance aware, or artifact suppressive. Hence, they rely upon intense postprocessing, which can eventually distort minute details while increasing the computational complexity.

Data driven methods. Previous learning-based studies generally adopt supervised [12], semi-supervised [24], zero-shot [25], and unsupervised learning [26] for solving low light enhancement problems.

Usual supervised methods focus on solving the low-light enhancement problem through an end-to-end approach or by using theoretical schemes such as retinex decomposition. In the first category, researchers propose stable networks and customized loss functions [3, 27, 9, 28, 29, 30], and in the second, two different objectives for reflectance and illumination are solved using novel architectures [31, 32, 33].

The study by Yang *et al.* [24] incorporates semi-supervised learning to perform image enhancement. Their work focuses on band learning from the input images, followed by decomposition and linear transformation. Zero-shot approaches focus on reducing label dependency and propose different approximation strategies. Zero-DCE [25] and Zero-DCE++ [34] obtain enhanced images by estimating multiple tone-curves from the input images. However, the computational burden is higher for these approaches than for other methods. EnlightenGAN [26] offers an unsupervised solution through an adversarial process but may lack stable generalization performance.

3 Atmospheric component learning

Prevalent theoretical methods regarding low-light enhancement come with several challenges, such as multiple-variable optimization and dependency on priors that lack diverse applicability. Our study addresses the above challenges and presents a prior-independent single variable optimization scheme using semi-supervised learning. We first apply the inversion operation on the low-light images. As a result, the transformed images inherit almost similar statistical properties to the hazy natural images [1]. Additionally, they also take in ‘sort of’ similar appearances to hazy images, thus enabling the possibilities to explore the effect of traditional image haze distribution equation (1) in this setup.

$$I(x) = J(x)t(x) + A(x)(1 - t(x)). \quad (1)$$

Here, $I(x)$ is the observed hazy image, $J(x)$ is the image we want to recover, $t(x)$ is the transmission component, and $A(x)$ is the global ambient component.

To integrate [10] onto the low light enhancement problem, we first invert our low-light input image $L(x)$ and the resultant image $1 - L(x)$, which is the ‘hazy image’, for this problem. The hazy $I(x)$ image is replaced by $1 - L(x)$, which will be denoted as $I'(x)$. Likewise, the recovered bright image $B(x)$ can be inverted to produce an enhanced low-light image, resulting in a simple variable replacement of equation (1) $I'(x) = B(x)t(x) + A(x)(1 - t(x))$. If we solve for $B(x)$, we have the following.

$$B(x) = \frac{1}{t(x)}I'(x) - A(x)\frac{1}{t(x)} + A(x). \quad (2)$$

In previous works, certain assumptions to solve the above equation (2) were made. For example, earlier studies typically set transmission information to be constant over the entire environment. This assumption leads to the optimization of a single variable $A(x)$; however, it is not practical for many lighting conditions. On the other hand, prior dark channels/bright channels are extracted in some works to obtain closed-form solutions for equation (1). The effectiveness of these practices suffer due to fluctuating transmission and ambient variables. Therefore, it is necessary to consider both of them to enable the best possible recovery of the given image. Accordingly, we adopt the following expression to solve over the training procedure:

$$B(x) = h(x)(I'(x) - 1) + c. \quad (3)$$

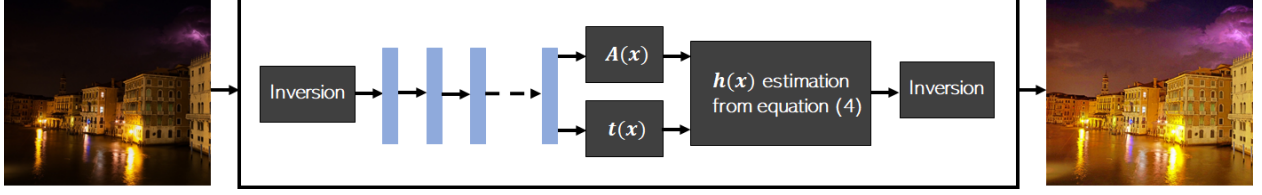


Figure 2: This picture depicts the network schematic of the proposed study. Here, we perform image inversion in the beginning and end to simulate hazy image. Inside the network, the atmospheric components of equation (4) is approximated by semi-supervised training and the reformulated hazy equation (3) is solved before the inversion.

$$h(x) = \frac{\frac{1}{t(x)}(I'(x) - A(x)) + (A(x) - c)}{I'(x) - 1}. \quad (4)$$

We have taken some algebraic liberties to formulate $h(x)$ in equation (3). With $h(x)$ formulated as in (4), the hazy equation (2) can be approximated to equation (3), where c is constant and $h(x)$ is the atmospheric component that combines the input image, transmission information, and ambient information. We set $c = 1$ to transform the negative result from the left part of the equation into a bounded positive value.

In the following subsection, we propose semi-supervised learning for approximating $h(x)$. Equation (3) is solved using non-trainable layers inside the semi-supervised trained network before sending $B(x)$ to the loss layer (see fig. 2). In this way, we can learn the effect of the ambient factors for the given image.

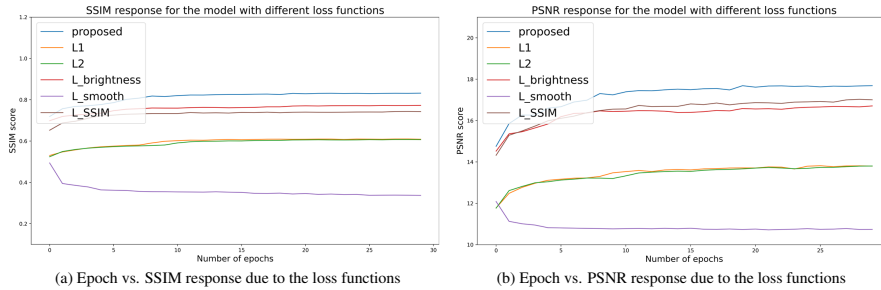


Figure 3: Here we show the response for the each loss functions used in our work. Under the same initialization, proposed combined loss-function avails better SSIM and PSNR response than the individual loss functions.

3.1 Validation metric for semi-supervised learning

The proposed semi-supervised learning starts with a few hundred images with ground truths. After the initial training, new images without ground truths can be added to the training set by using the results from the initially trained network as ground truths. Naively, it may seem that the new training images will simply reinforce the current state of the network. However, this is avoided when we use a multi-objective loss function with smoothness and brightness costs so that a network response that is the same as the ground truth does not necessarily produce the minimum loss. Likewise, we can choose only the images that produce an ‘objectively correct’ network response. The correctness of the network response image can be validated by image quality assessment metrics that are not based on the ground-truth reference image.

For this study, we used the GLADNet dataset [9] for training and the NIQE metric to validate the correctness of the network response. NIQE has been used in many previous studies [25, 3, 31] for quantitative comparison of image quality. The GLADNet dataset has ground-truth reference images, of which only 500 were used in our study.

We first took 500 random images from the GLADNet dataset with their corresponding ground truths. The NIQE scores of the 500 ground-truth images were then computed. Since these images have proper light distribution, their NIQE scores are much lower than their low light counterparts. The average of the precomputed NIQE scores of the preselected reference image is denoted as N_a . The network was trained with this small subset until primary local minima are reached for the network.

R_1 denotes the large set of images without ground-truth images. The network response images from R_1 are computed as \hat{R}_1 , and NIQE scores for \hat{R}_1 images are calculated. To select the subsequent images to be included for retraining, we

only include images that have response images with *NIQE* scores that are very near the precomputed value N_a . Thus, the results from unlabeled images must be validated by the desired *NIQE* score before inclusion in the training set.

If m images from \hat{R}_1 pass the *NIQE* metric validation, the training set will be updated with $500 + m$ paired images, of which 500 will have true ground truth and m will have images from \hat{R}_1 as acting ground truths. In this way, we start the retraining with our mixed labels and repeat until we update the parameter space with the whole GLADNet dataset of 5000 samples. We experimented with different starting subsets from the GLADNet dataset but did not observe any significant deviance from the reported result. Up to 5 rounds of retraining was required to cover the entire dataset with high *NIQE* scores.

Because the new training images with acting ground truths are validated with the *NIQE* metric, the resultant network produces desirable *NIQE* scoring images as a side effect. The target loss function itself does not include the *NIQE* score in its formulation, which allows *NIQE* to be a viable validation metric. The specifics of the loss function are introduced in the next subsection.

3.2 Loss function

Inferences from typical end-to-end models may contain artifacts such as over-smoothing, lack of contrast, or traces of convolution operations. Hence, some approaches rely on hand-crafted post-inference tuning as an extension of the method. To avoid such manual operations, we propose a combined loss function with the aims of reducing blurry edges, suppressing noise, and producing adaptive contrast independent of the domain while achieving high image quality metric scores.

We experimented with different loss function setups, and the following loss function is proposed.

$$L_{total} = \lambda_1 L_1 + \lambda_2 L_{brightness} + \lambda_3 L_{smooth} + L_{SSIM}. \quad (5)$$

We started with the L_1 loss function, which is the distance between the ground truth and the prediction image. To go further, we propose $L_{brightness}$ loss to introduce more light information during prediction. The equations for the L_1 and $L_{brightness}$ are as follows:

$$L_1 = \frac{1}{n} \sum_{j=1}^n |y_g - y_p|. \quad (6)$$

$$L_{brightness} = \frac{1}{n} \sum_{j=1}^n |y_g^{\gamma_1} - y_p^{\gamma_2}|. \quad (7)$$

Here, y_g is the ground truth, and y_p is the prediction, which is universal for both supervised pre-training and semi-supervised iterations. For the $L_{brightness}$ loss function, $y_g^{\gamma_1}$ and $y_p^{\gamma_2}$ are the gamma-corrected ground truths and the predictions respectively. Our $L_{brightness}$ loss function first darkens the predicted image and brightens the corresponding labels through gamma correction and then measures the L_1 distance between them.

The L_{smooth} loss measures the distance between the prediction and the corresponding smoothed label image by median, Gaussian, consecutive upsampling and downsampling.

$$L_{smooth} = \frac{1}{n} \sum_{j=1}^n |y_g^{smooth} - y_p|. \quad (8)$$

If L_{smooth} is the only loss function for the overall training process, it will constrain the parameter space to infer a smoothed-out enhanced image. In many of the previous methods, smoothing was obtained through postprocessing in order to reduce the remaining noise. Here instead, we crafted the loss function to learn smoothing during training.

The final component is the SSIM loss, which constraints the parameter space to adapt to image metric performance.

$$L_{SSIM} = \frac{1}{n} \sum_{j=1}^n 1 - SSIM(y_g, y_p). \quad (9)$$

The L_1 loss, $L_{brightness}$ loss for brighter prediction, noise-suppressing L_{smooth} , and the L_{SSIM} loss together aid in achieving overall perceptual and structural fidelity. To successfully inject the influences of all the loss functions into the architecture, we empirically tuned the parameters to $\lambda_1 = 0.35$, $\lambda_2 = 0.5$, and $\lambda_3 = 0.15$. For the gamma correction, $\gamma_1 = 0.85$, and $\gamma_2 = 1.15$ were chosen through the convex sum. Fig. 3 shows the results of an identically initialized network with individual loss functions L_{total} , L_1 , L_2 , $L_{brightness}$, L_{smooth} , and L_{SSIM} and the proposed combined loss function. The efficacy of the proposed loss function in comparison to each loss function is shown.

4 Experiments

In this section, we demonstrate the performance of the proposed method in comparison to 11 contemporary studies. In the following, we present the experimental settings and then show the qualitative and quantitative evaluation on six widely used datasets over 6 different metrics.

4.1 Experimental setup

In our training process, we use the Adam optimizer with a learning rate of 0.0001. We utilize the learning rate decay from the original TensorFlow library, where we monitor the validation SSIM to decay the learning rate. Over the total training time, we used a batch size of 16 and normalized all images between 0 and 1. We adopt the usual data augmentation procedure for the overall training procedure. In our training setup, we did not fragment the training images to smaller patches. Additionally, we keep the image sizes to be their original size during the training process. We adopt the training dataset from the GLADNet dataset. This dataset contains 5000 low-light images with their corresponding labels. The images in the dataset are not limited to any specific environment or class instances and contain both indoor and outdoor photos taken in daylight or nighttime of humans, animals, and natural images.

4.2 Comparison

Datasets. We apply our testing procedure to six datasets: LIME [35], LOL [34], MEF [36], NPE [19], DICM [37], and VV [38]. Here, only the LOL dataset contains the ground truths for the test images, and the rest are unpaired. However, the LOL dataset only contains indoor scenes. The diversity of the other datasets is similar to that of the GLADNet dataset.

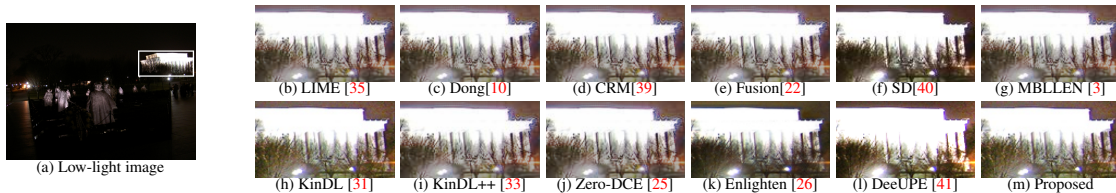


Figure 4: This figure compares the night-time image reconstruction performance. From the figure, we can see the presence of noise and the trace of convolution in many of the restored images. In comparison to other methods, proposed approach can recover the scene without perturbing the homogeneity of the foreground and background (for best view, zoom-in is recommended).

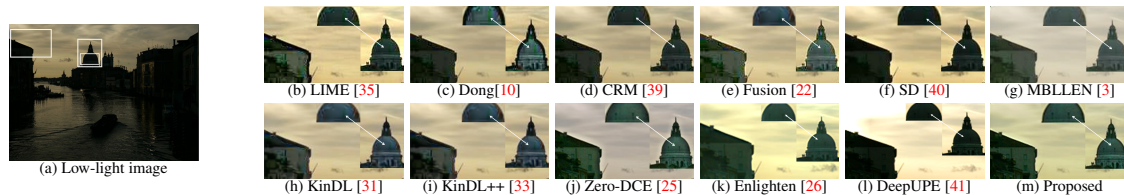


Figure 5: This figure shows the typical low light image enhancement comparison. Here, we highlight the window recovery for the dome. The propose approach is one of the few methods that can recover the windows while achieving desired lighting condition. Additionally, we see proposed study can preserve the ambient contrast by suppressing the over-whitening (for best view, zoom-in is recommended).

Compared studies. For comparison, we use the following methods: Dong et al. [10], LIME [35], CRM [39], fusion [22], semi-decoupled [40], MBLLEN [3], KinDL [31], KinDL++ [33], EnlightenGAN [26], DeepUPE [41], and Zero-DCE [25]. Since most test images do not come with corresponding ground truths, we use no-reference metrics such as PIQE, NIQE, and BRISQUE. Here, NIQE stands for the Naturalness Image Quality Evaluator, which signifies the deviations of statistical regularities for a given image without any reference. Similarly, PIQE inversely corresponds to the perceptual quality of the given image. BRISQUE also operates blindly and utilizes locally normalized luminance coefficients to compute the image quality. Tables 1, 2 and 3 show that our method achieves state-of-the-art or comparable performances for the given datasets and produces the best average score across all datasets.

From figures 4 and 5, we can see the restoration difference between the proposed study and the compared studies. The studies used for comparison show the traces of convolution on the edge line, noisy reconstruction, color distortion, and

Table 1: Perception Image Quality Evaluator (PIQE) comparison between nine low light enhancement methods on six different datasets. Best score is in bold and second best is underlined.

Method/Dataset	VV[38]	DICM[37]	LIME[35]	LOL[34]	MEF[36]	NPE[19]	Average
LIME[35]	19.8520	16.3735	12.6429	13.6715	16.8422	13.7836	15.5276
Dong et al.[10]	13.2391	13.9523	14.5912	19.1315	18.4940	14.4011	15.6348
MBLLEN[3]	11.5750	16.1056	16.1573	13.1625	20.3220	13.6689	15.1652
CRM[39]	12.2987	15.6655	13.1111	19.1352	18.4965	13.1257	15.3054
Fusion[22]	<u>9.0956</u>	15.6556	12.1613	17.8952	19.9009	13.5352	14.7073
KinDL[31]	10.7151	11.9790	12.8772	<u>9.3091</u>	11.6322	16.3012	12.1356
KinDL++[33]	10.7045	<u>7.9980</u>	13.5777	8.7117	9.5811	16.1812	11.1257
Semi-Decoupled[40]	9.3511	17.587	12.5561	27.7175	22.6213	16.5653	11.7347
Zero-DCE[25]	9.6766	8.1825	9.6177	11.3682	7.6688	10.9502	<u>9.5773</u>
EnlightenGAN [26]	9.9112	12.2223	13.1718	11.9347	15.4127	13.0161	12.6030
DeepUPE [41]	11.3748	9.6465	14.2783	13.0920	17.3246	17.0602	13.8321
Proposed	7.0877	7.5725	<u>10.0965</u>	11.2002	7.0011	<u>11.0311</u>	7.8169

Table 2: Naturalness Image Quality Evaluator (NIQE) comparison between eleven low light enhancement methods on six different datasets. The best score is in bold and the second best is underlined.

Method/Dataset	VV[38]	DICM[37]	LIME[35]	LOL[34]	MEF[36]	NPE[19]	Average
LIME[35]	3.9788	3.5009	4.9526	4.1368	4.1155	<u>3.4458</u>	<u>4.0217</u>
Dong et al.[10]	4.2628	4.2002	4.2021	3.8971	4.6315	3.8263	4.1700
MBLLEN[3]	3.5721	4.9279	4.3491	3.9303	3.2391	3.3416	3.8933
CRM[39]	3.7216	4.2148	4.3552	<u>3.1583</u>	4.7578	4.3230	4.0884
Fusion[22]	3.8535	3.3375	3.4659	3.2639	3.9106	3.3991	3.5384
KinDL[31]	<u>3.4269</u>	3.5401	4.3527	3.0722	2.7614	3.9581	3.5185
KinDL++[33]	3.5726	3.9136	4.1922	3.8945	3.2907	4.3072	3.8618
Semi-Decoupled[40]	4.8923	4.1358	5.3796	5.8426	5.5946	4.2899	6.5266
Zero-DCE[25]	10.504	11.7541	14.1206	7.3112	12.1316	10.7102	12.8393
EnlightenGAN[26]	3.9012	3.8521	4.4123	3.9751	4.1725	3.7451	5.9732
DeepUPE[41]	4.2258	3.9651	5.0751	4.6723	3.8122	4.0943	4.3052
Proposed	2.7642	<u>3.4239</u>	<u>3.7071</u>	3.3188	<u>3.0102</u>	3.8009	3.3375

Table 3: Blind/Referenceless Image Spatial Quality Evaluator (BRISQUE) comparison between nine low light enhancement methods on six different datasets. Best score is in bold and second best is underlined.

Method/Dataset	VV[38]	DICM[37]	LIME[35]	LOL[34]	MEF[36]	NPE[19]	Average
LIME[35]	27.5223	36.9602	25.8193	25.8509	38.9459	21.9541	29.5087
Dong et al.[10]	28.5563	45.5648	27.0681	27.9744	40.6047	26.6699	32.7413
MBLLEN[3]	24.0018	25.4718	27.4972	13.8857	27.6337	20.8256	40.1556
CRM[39]	27.0305	34.8725	26.8219	21.5269	38.0785	23.0998	28.5716
Fusion[22]	25.8686	35.9418	26.9049	<u>19.9002</u>	38.7504	22.8034	28.3615
KinDL[31]	23.1707	32.4027	32.3042	26.9681	33.3069	<u>20.1546</u>	28.0512
KinDL++[33]	<u>22.8755</u>	31.1161	37.4435	22.2963	32.9189	20.4419	27.8487
Semi-Decoupled[40]	24.2539	33.7456	26.6086	38.4748	35.5634	22.3599	30.1677
Zero-DCE[25]	34.2122	<u>23.6767</u>	<u>22.0031</u>	32.0853	25.2623	25.6566	<u>27.1694</u>
EnlightenGAN [26]	25.1723	34.9652	27.4341	30.6912	<u>21.4321</u>	26.8712	27.7651
DeepUPE[41]	28.3457	36.2712	26.1122	23.1612	23.7512	31.4325	28.6123
Proposed	22.4367	17.0272	19.0254	32.2238	13.3232	15.3297	21.5610

overly contrast stretching in the given restored image. Additionally, we have highlighted the specific portion for all methods to demonstrate the restoration complexities. For example, in figure 5, only our approach and Zero-DCE [25] can successfully recover the cathedral’s dome with its windows, while other methods leave it without any window and show noisy restoration. These visual results demonstrate that the proposed method can restore low light images with minute details while preserving the naturalness of the content while exhibiting as much noise suppressive behavior as possible. Additionally, better and competitive metric performances also show our method’s effectiveness in diverse datasets.

4.3 Identity preservation for image restoration

Low-light image enhancement is a vital and mandatory postprocessing in smartphones cameras to ensure visual clarity and aesthetics. Recent trends show that low-light camera performance is an acid test for smartphone cameras. The proposed network was able to suppress noise, preserve details, restore instance-aware colors, and maintain overall

fidelity. We have validated our network’s through both qualitative visual performance and quantitative evaluations for six popular datasets.

However, one major issue with deep-learning studies is dataset bias. Due to this, some studies show gender bias during the inference stage. In figure 6, KinDL [31] and KinDL++ [33] identify the woman in the low-light image but also infers lipstick on the enhanced image of the woman, which contradicts the low-light face without lipstick mark. As the unsupervised methods promises to be unbiased, Zero-DCE[25] and EnlightenGAN[26] study show no such reconstruction. Our network also preserves the woman’s actual identity and does not show any assertion bias for the woman, even with semi-supervised training.

Furthermore, in the same figure, our network also captures the background people and preserves the human face intact during inference. In comparison, the compared methods interpolate the background people’s faces as humanoid face blobs and this can significantly damage person recognition performance. In the third row of the figure 6, our network can successfully infer the human face without any out-of-domain artifacts or damaging the person’s identity. These minute performance gains can significantly affect the efficacy of surveillance systems or general person identification-related applications.

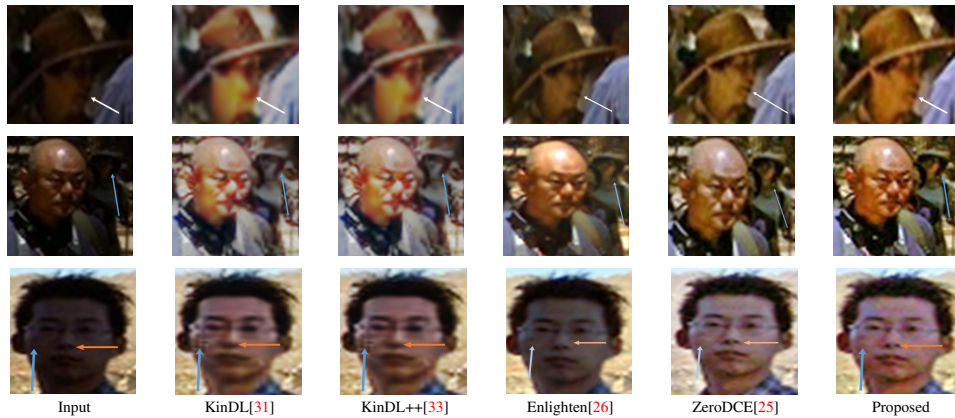


Figure 6: Demonstration of identity preservation. The previous data-driven methods assign the lipstick marking on the woman, but lipstick is not present in the original images. The proposed approach is free from such bias, even though it was semi-supervised. In the second row, the proposed method can recover the background faces context-coherently, where other data-driven methods tend to blend the faces with the environment light. In the last row, the proposed approach faithfully reconstructs the person’s nose as with other unsupervised methods. Again, previous data-driven method’s noses differ significantly from the low-light face (for best view, zoom-in is recommended).

In the end, it is difficult to quantify a network’s limitations on these biases; how many different biases are present, is the data set or the network more liable for the bias, or what is the guarantee that it will be bias free in real-life scenarios? Despite all of these challenges, our study presents a lightweight network with only 11k parameters and shows significant improvements through semi-supervised learning. At least for these examples, it was able to maintain person’s identity and did not assert gender bias to achieve instance-aware low-light enhancement performances.

5 Conclusion

This study aims to deliver an effective solution for low-light enhancement by learning the atmospheric components from the given image. Primarily, atmospheric elements allow us to enhance low light images with minimal artifacts. Furthermore, we address the low-light image enhancement through the semi-supervised approach to reduce the need for ground-truth paired images and dataset bias. To establish the overall scheme, we propose a combined loss function that applies the necessary constraint to enable the network to learn sophisticated features from the training domain. Our experimental results show that the proposed scheme can restore low-light images with high fidelity and achieve satisfactory performance in six different datasets when compared to eleven state-of-the-art studies. We also discuss our concerns about the biases influencing the deep network’s performance during image restoration. In the future, we aim to focus on more elegant learning approaches and to increase generalization ability for image restorations, while augmenting their performances in diverse vision applications. Additionally, we plan to work on analyzing biases within deep computational photography applications.

References

- [1] Wencheng Wang, Xiaojin Wu, Xiaohui Yuan, and Zairui Gao. An experiment-based review of low-light image enhancement methods. *IEEE Access*, PP:1–1, 05 2020. 1, 2, 3
- [2] Sungmin Lee, Seokmin Yun, Ju-Hun Nam, Chee Won, and Seung-Won Jung. A review on dark channel prior based image dehazing algorithms. *EURASIP Journal on Image and Video Processing*, 2016, 01 2016. 1
- [3] Jianhua Wu Feifan Lv, Feng Lu and Chongsoon Lim. Mblen: Low-light image/video enhancement using cnns. *British Machine Vision Conference*, 2018. 1, 3, 4, 6, 7
- [4] Zia-Ur Rahman, Daniel Jobson, and Glenn Woodell. A multiscale retinex for color rendition and dynamic range compression. *Proc. SPIE*, 2847:183–191, 11 1996. 1, 3
- [5] Daniel Jobson. Retinex processing for automatic image enhancement. *Journal of Electronic Imaging*, 13:100, 01 2004. 1, 3
- [6] Wenjing Wang, Wenhan Yang, and Jiaying Liu. Deep retinex decomposition for low-light enhancement. 08 2018. 1, 2, 3
- [7] S.G. Narasimhan and S.K. Nayar. Contrast restoration of weather degraded images. *IEEE Transactions on Pattern Analysis and Machine Intelligence*, 25(6):713–724, 2003. 2
- [8] Ancuti Codruta, Cosmin Ancuti, Christophe Vleeschouwer, and Philippe Bekaert. Color balance and fusion for underwater image enhancement. *IEEE Transactions on Image Processing*, PP:1–1, 10 2017. 2
- [9] Wenjing Wang, Wenhan Yang, and Jiaying Liu. Gladnet: Low-light enhancement network with global awareness. pages 751–755, 05 2018. 2, 3, 4
- [10] Xuan Dong, Guan Wang, Yi Pang, Weixin Li, Jiangtao Wen, Wei Meng, and Yao Lu. Fast efficient algorithm for enhancement of low lighting video. In *2011 IEEE International Conference on Multimedia and Expo*, pages 1–6. IEEE, 2011. 2, 3, 6, 7
- [11] Kaiming He, Jian Sun, and Xiaoou Tang. Single image haze removal using dark channel prior. *IEEE Trans. Pattern Anal. Mach. Intell.*, 33:2341–2353, 01 2011. 2, 3
- [12] Xueyang Fu, Delu Zeng, Yue Huang, Xinghao Ding, and X.-P Zhang. A variational framework for single low light image enhancement using bright channel prior. pages 1085–1088, 12 2013. 2, 3
- [13] Xiaojie Guo, Li Yu, and Haibin Ling. Lime: Low-light image enhancement via illumination map estimation. *IEEE Transactions on Image Processing*, PP:1–1, 12 2016. 3
- [14] Wu Zhihong and Xiao Xiaohong. Study on histogram equalization. 10 2011. 3
- [15] Laurence Krpoun-Meylan and Sabine Süsstrunk. High dynamic range image rendering with a retinex-based adaptive filter. *IEEE transactions on image processing : a publication of the IEEE Signal Processing Society*, 15:2820–30, 10 2006. 3
- [16] Ming-rong Wang and Shu-qing Jiang. Image enhancement algorithm combining multi-scale retinex and bilateral filter. 01 2015. 3
- [17] Agustien Mulyantini and Heung-Kook Choi. Color image enhancement using a retinex algorithm with bilateral filtering for images with poor illumination. *Journal of Korea Multimedia Society*, 19:233–239, 02 2016. 3
- [18] Dan Zhu, Guannan Chen, Pablo Navarrete Michelini, and Hanwen Liu. Fast image enhancement based on maximum and guided filters. pages 4080–4084, 09 2019. 3
- [19] Shuhang Wang, Jin Zheng, Hai-Miao Hu, and Bo Li. Naturalness preserved enhancement algorithm for non-uniform illumination images. *IEEE transactions on image processing : a publication of the IEEE Signal Processing Society*, 22, 05 2013. 3, 6, 7
- [20] Yurui Ren, Zhenqiang Ying, Thomas Li, and Ge Li. Lecarm: Low-light image enhancement using camera response model. *IEEE Transactions on Circuits and Systems for Video Technology*, PP:1–1, 04 2018. 3
- [21] Zhenqiang Ying, Ge Li, and Wen Gao. A bio-inspired multi-exposure fusion framework for low-light image enhancement. 11 2017. 3
- [22] Zhenqiang Ying, Ge Li, Yurui Ren, Ronggang Wang, and Wenmin Wang. A new image contrast enhancement algorithm using exposure fusion framework. pages 36–46, 07 2017. 3, 6, 7
- [23] Alexander Toet. Colorizing single band intensified nightvision images. *Displays*, 26:15–21, 01 2005. 3
- [24] Wenhan Yang, Shiqi Wang, Yuming Fang, Yue Wang, and Jiaying Liu. From fidelity to perceptual quality: A semi-supervised approach for low-light image enhancement. pages 3060–3069, 06 2020. 3

- [25] Chunle Guo, Chongyi Li, Jichang Guo, Chen Change Loy, Junhui Hou, Sam Kwong, and Runmin Cong. Zero-reference deep curve estimation for low-light image enhancement. In *Proceedings of the IEEE/CVF Conference on Computer Vision and Pattern Recognition*, pages 1780–1789, 2020. [3](#), [4](#), [6](#), [7](#), [8](#)
- [26] Yifan Jiang, Xinyu Gong, Ding Liu, Yu Cheng, Chen Fang, Xiaohui Shen, Jianchao Yang, Pan Zhou, and Zhangyang Wang. Enlighten: Deep light enhancement without paired supervision. *IEEE Transactions on Image Processing*, PP:1–1, 01 2021. [3](#), [6](#), [7](#), [8](#)
- [27] Kin Gwn Lore, Adedotun Akintayo, and Soumik Sarkar. Llnet: A deep autoencoder approach to natural low-light image enhancement. *Pattern Recognition*, 61, 11 2015. [3](#)
- [28] Minfeng Zhu, Pingbo Pan, Wei Chen, and Yi Yang. Eemefn: Low-light image enhancement via edge-enhanced multi-exposure fusion network. *Proceedings of the AAAI Conference on Artificial Intelligence*, 34:13106–13113, 04 2020. [3](#)
- [29] Kun Lu and Lihong Zhang. Tbefn: A two-branch exposure-fusion network for low-light image enhancement. *IEEE Transactions on Multimedia*, PP:1–1, 11 2020. [3](#)
- [30] Seokjae Lim and Wonjun Kim. Dslr: Deep stacked laplacian restorer for low-light image enhancement. *IEEE Transactions on Multimedia*, PP:1–1, 11 2020. [3](#)
- [31] Yonghua Zhang, Jiawan Zhang, and Xiaojie Guo. Kindling the darkness: A practical low-light image enhancer. pages 1632–1640, 10 2019. [3](#), [4](#), [6](#), [7](#), [8](#)
- [32] Qian Gao, Pengyu Liu, Shanji Chen, and Kebin Jia. A zero-dce-based low-light image enhancement algorithm for urban roads. pages 356–360, 10 2020. [3](#)
- [33] Yonghua Zhang, Xiaojie Guo, Jiayi Ma, Wei Liu, and Jiawan Zhang. Beyond brightening low-light images. *International Journal of Computer Vision*, 129, 04 2021. [3](#), [6](#), [7](#), [8](#)
- [34] Chongyi Li, Chunle Guo, and Chen Change Loy. Learning to enhance low-light image via zero-reference deep curve estimation. *CoRR*, abs/2103.00860, 2021. [3](#), [6](#), [7](#)
- [35] Xiaojie Guo, Li Yu, and Haibin Ling. Lime: Low-light image enhancement via illumination map estimation. *IEEE Transactions on Image Processing*, PP:1–1, 12 2016. [6](#), [7](#)
- [36] Chulwoo Lee, Chul Lee, Young-Yoon Lee, and Chang-Su Kim. Power-constrained contrast enhancement for emissive displays based on histogram equalization. *IEEE transactions on image processing : a publication of the IEEE Signal Processing Society*, 21:80–93, 06 2011. [6](#), [7](#)
- [37] Chulwoo Lee, Chul Lee, and Chang-Su Kim. Contrast enhancement based on layered difference representation of 2d histograms. *IEEE transactions on image processing : a publication of the IEEE Signal Processing Society*, 12 2013. [6](#), [7](#)
- [38] Chongyi Li, Chunle Guo, Linghao Han, Jun Jiang, Ming-Ming Cheng, Jinwei Gu, and Chen Change Loy. Lighting the darkness in the deep learning era. *CoRR*, abs/2104.10729, 2021. [6](#), [7](#)
- [39] Zhenqiang Ying, Ge Li, Yurui Ren, Ronggang Wang, and Wenmin Wang. A new low-light image enhancement algorithm using camera response model. 10 2017. [6](#), [7](#)
- [40] Shijie Hao, Xu Han, Yanrong Guo, Xin Xu, and Meng Wang. Low-light image enhancement with semi-decoupled decomposition. *IEEE Transactions on Multimedia*, 22(12):3025–3038, 2020. [6](#), [7](#)
- [41] Ruixing Wang, Qing Zhang, Chi-Wing Fu, Xiaoyong Shen, Wei-Shi Zheng, and Jiaya Jia. Underexposed photo enhancement using deep illumination estimation. In *The IEEE Conference on Computer Vision and Pattern Recognition (CVPR)*, June 2019. [6](#), [7](#)